Version: Accepted author manuscript
Published in: Coastal Sediments 2019 Conference proceedings, pp. 1693-1707
Published version: doi: 10.1142/9789811204487_0146

SCALE EXPERIMENTS ON AEOLIAN DEPOSITION AND EROSION PATTERNS CREATED BY BUILDINGS ON THE BEACH

DAAN W. POPPEMA[1], KATHELIJNE M. WIJNBERG[1], JAN P.M. MULDER[1] & SUZANNE J.M.H. HULSCHER[1]

1. *Water Engineering and Management, University of Twente, P.O. Box 217, 7500 AE Enschede, The Netherlands. d.w.poppema@utwente.nl*

Abstract: Worldwide, buildings are present at the beach and in the dunes for recreation or habitation. Their presence can affect the beach-dune development, because they affect the airflow and Aeolian sediment transport in their surroundings. This might eventually have repercussions for coastal safety. We start examining these effects by studying the local sedimentation and erosion patterns around buildings. Hereto, we placed scale models of buildings on the beach. The sedimentation and erosion patterns around the models were measured using structure-from-motion photogrammetry. In general, the air flow around bluff bodies like buildings forms a horseshoe vortex. This creates deposition and erosion patterns in a horseshoe shape. For nearly all scale models, the upwind part and downwind tails of the horseshoe showed deposition. The horseshoe deposition at the building sides was sometimes visible, also depending on building orientation. Frequently, smaller erosion and/or deposition areas also developed between the horseshoe deposition and the building.

Introduction

Worldwide, urbanization and a demand for recreation have led to buildings being built at the beach-dune interface. This occurs in the form of houses for recreational seasonal use or permanent habitation, hotels, restaurants and commercial stalls (Jackson & Nordstrom, 2011). In the Netherlands, there is an increasing demand for these buildings and a shift to more year-round present restaurants (Hoonhout & Waagmeester, 2014). A similar trend is found in other countries, both for coastal tourism in general (Hall, 2001; Moreno & Amelung, 2009) and the number of buildings at the beach-dune interface (Schlacher et al., 2008; Malavasi et al., 2013).

All these buildings alter the wind field and the related wind-driven sediment transport in their vicinity. They can decrease the wind speed and promote sedimentation in their surroundings, for instance in front of buildings and at the lee side of buildings (Nordstrom, 2000; Jackson & Nordstrom, 2011; Smith et al., 2017). Conversely, air flow in between buildings can also be accelerated, causing local erosion and increased sediment transport (Nordstrom, 2000; Jackson & Nordstrom, 2011). The same effect can be seen under houses on pilings, where a scour zone can commonly be found (Nordstrom & James, 1985; Jackson & Nordstrom, 2011). Furthermore, an increased turbulent intensity in the wake of

houses can promote an increase in sediment transport (Smith et al., 2017). Continuous lines of buildings can also form a barrier for sediment transport, separating dunes from their beach or foredune sources and thereby causing fetch segmentation (Jackson & Nordstrom, 2011; Smith et al., 2017).

Aeolian sediment transport from the beach to the dune zone is essential for long-term coastal safety. Dunes protect the hinterland against flooding and provide a high ground to live on. They need an influx of sand to balance natural dune erosion caused by storms (Morton et al., 1994; Keijsers, 2015), to keep step with (relative) sea level, and to compensate for the expected increase in hydrodynamic erosion due to climate change (Carter, 1991; Keijsers, 2015; De Winter & Ruessink, 2017).

The combination of 1) a worldwide presence and demand for buildings at the beach-dune interface; 2) their effect on the Aeolian sediment transport and beach-dune morphology; and 3) the importance of Aeolian sediment transport for coastal safety, necessitates a proper understanding of how buildings on the beach-dune interface affect their environment. The first step in this research is to describe the local erosion and sedimentation patterns around a building and define generic patterns from these observations. To determine these erosion and deposition patterns, scale experiments on the beach will be used with various configurations of buildings. The first of these field experiments were conducted in the fall of 2018, examining single buildings in isolation, placed directly on the ground.

In this paper we first describe the air flow around buildings and the expected sedimentation and erosion patterns (the theory section). Next, in the methodology we specify the set-up of our experiments. The results section gives a qualitative overview of the different types of sedimentation and erosion patterns that occurred during the experiment. Finally, the paper ends with a discussion and conclusion.

Theory

The wind around a bluff object like a building forms a horseshoe vortex (Hunt, 1971; Peterka et al., 1985; fig. 11 Martinuzzi & Tropea, 1993). A stagnation zone exists around ⅔ to ¾ of the building height. Above this zone, wind is diverted upward and to the sides. Below this zone, the pressure caused by the wind profile diverts the wind downward and to the sides (Peterka et al., 1985). These upward and sideward flows separate from the front of the building at the edges. Upwind of the building, the increased pressure and downward flow cause a reverse flow close to the ground. This creates a rotating vortex in front of the building, that is wrapped around the building in a horseshoe shape (Hunt, 1971; Peterka et al., 1985; Martinuzzi & Tropea, 1993).

The separated flow over the building edges can reattach at the top and side of the building before it reaches the back of the building. Whether it reattaches depends on the building's length-to-width and length-to height ratio and on the turbulent intensity (Hunt, 1971; Peterka et al., 1985). If flow reattachment does not occur, the flow at the side and top of the building forms one big recirculation cell with the flow behind the building. If flow reattachment occurs, a separate recirculation cell is formed behind the downwind edges of the building. Within the recirculation cell, two standing vortices occur at the building corners, forming an arch behind the building (Peterka et al., 1985; Martinuzzi & Tropea, 1993).

Deposition and erosion patterns around buildings are the direct effect of these wind flows and often follow the horseshoe shape. Although little research exists on the Aeolian erosion and deposition of sand around buildings, multiple experiments on the deposition and erosion of snow were conducted (Thiis & Gjessing, 1999; Oikawa & Tomabechi, 2000; Thiis, 2003; Liu et al., 2018). Although there are some differences with sand – most notably the lower density and cohesion of snow and the possibility of snow fall – the wind field and processes are similar, so these experiments still provide insight on the Aeolian erosion and deposition of sand around bluff bodies like buildings.

In field experiments on the snow drift around a cube with sides of 2.5 m, Thiis and Gjessing (1999) observed a deposition horseshoe. Following the nomenclature of figure 1, the upwind horseshoe deposition was clearly separated from the building front. The lateral horseshoe depositions were absent and the downwind horseshoe depositions were present. These downwind depositions, also called deposition tails, differed in length due to an oblique wind angle. Close to the building no (inner) deposition was observed. The lack of a downwind inner deposition was probably caused by the windspeed, that was too low to cause suspensive transport that could be blown over the cube. In a later study of Thiis (2003), downwind inner deposition developed especially after a stronger wind event (15 m/s). Lateral horseshoe depositions were again barely visible.

In other experiments, snow accumulation was observed around cubes under conditions of combined snow drift and snow fall. Using cubes of 0.5 m and wind speeds from 0.5 to 4.5 m/s, Liu et al. (2018) found that at low wind speed (1.5 m/s), a deposition horseshoe developed, touching the front of the building and the back corners. At 3.5 m/s, two elevation maxima developed upwind of the cube (so indicating upwind horseshoe deposition and upwind inner deposition). At 4.5 m/s, these areas were actually separated by an upwind erosion area. Upwind of the cube, Oikawa and Tomabechi (2000) found that the inner erosion depth and horseshoe deposition depth increased with wind speed (using 1m-sized cubes and day-averaged wind speeds from 1.5 to 5 m/s). Below the threshold velocity (4 m/s), wind speed also had a positive effect on the upwind inner deposition depth.

At the sides of the cube, Liu et al. observed that the distance between the cube and lateral horseshoe deposition increased from 1.5 to 3.5 m/s wind speeds, while the lateral horseshoe deposition disappeared completely at 4.5 m/s. Downwind op the cube, Liu et al. found a minimal amount of inner deposition at the lowest windspeed – possibly aided by the presence of snow fall – which became more significant at higher wind speeds. Oikawa and Tomabechi found not only downwind inner erosion and deposition directly behind the cube, but also downwind deposition further away (at more than twice the cube height away).

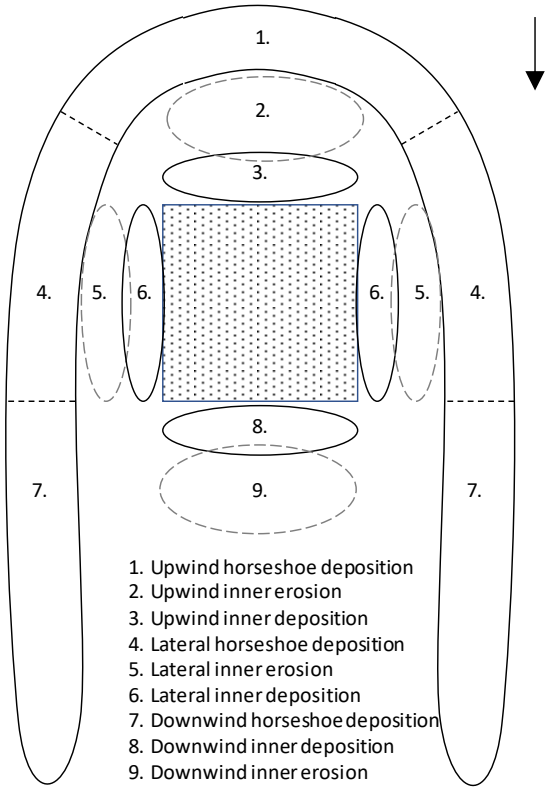

Figure 1: The locations and names of possible Aeolian erosion and deposition features around a cube or building.

Methodology

Scale models of buildings were placed at the beach to determine the Aeolian sedimentation and erosion patterns of sand around buildings (Fig. 2, Fig. 3). The scale models were cuboid stacks of cardboard boxes. These stacks varied in size

and shape, in order to determine the effect of building size and shape. The boxes used were 50x32x35 cm and the model length, width and height were varied between 1 and 4 boxes. Boxes were filled with a sand bag to prevent them from being blown away.

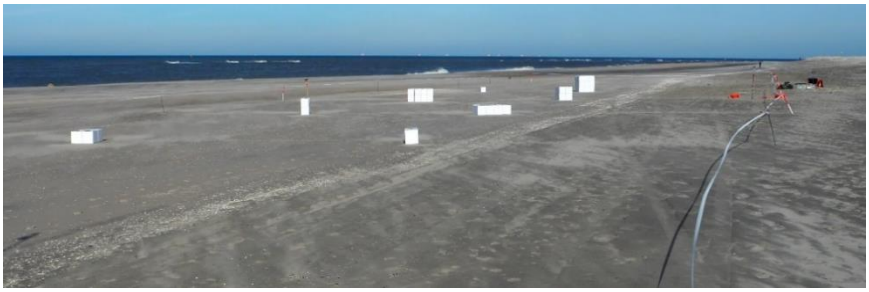

Figure 2: A photo of one of the set-ups, testing the effect of building width and height (12-10-2018)

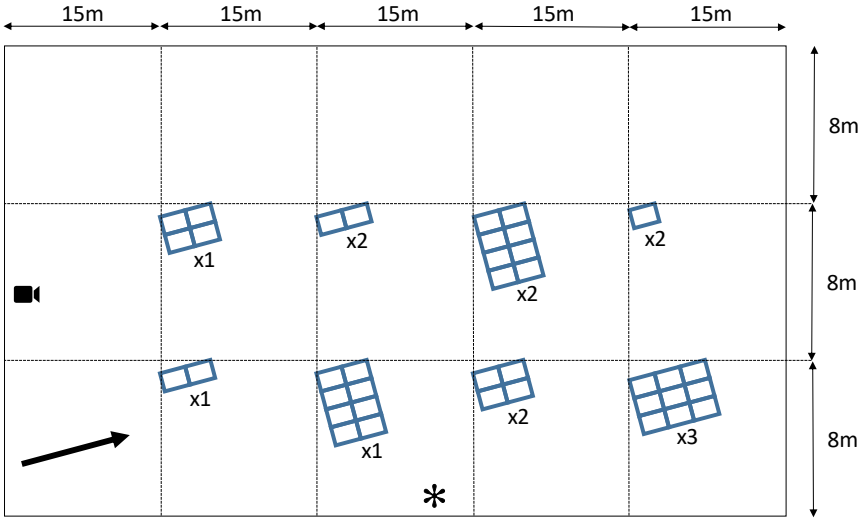

Figure 3: A sketch (not to scale) of the set-up shown in Figure 2. The arrow indicates wind direction, the camera icon the camera for the timelapse video, ✻ the Windsonic and Wenglors and x1/x2/x3 the number of boxes stacked upon each other

Field experiments at the beach were chosen over wind tunnel experiments, because field experiments allow to test under natural conditions and at a natural scale. Wind tunnels – while suitable for examining air flows around buildings – have difficulties simulating sediment transport and bed development. The problem here mainly concerns scaling and irreconcilable dimensionless numbers (White, 1996; Duthinh & Simiu, 2011), further complicated by the introduction of buildings. In addition, turbulent field conditions are notoriously difficult to

mimic in wind tunnels (Duthinh & Simiu, 2011), while simultaneously important for the flow structure around buildings (Peterka et al., 1985; Smith et al., 2017). Placing models at the beach allowed for using larger sizes than what could be tested in a wind tunnel (especially when considering configurations of multiple buildings). Nonetheless, some degree of scaling was applied in our field experiments (approximately a 1:10 to 1:3 scale) to make the set-up more flexible and manageable.

Scale models were placed at the beach in the morning, so that sedimentation and erosion patterns could develop during the day. They were oriented approximately perpendicular to the wind. Figure 2 and 3 show an example of the set-up. During the day, the wind speed and wind direction were measured at a 1s interval using a WindSonic 2D ultrasonic anemometer placed at a height of 1.8 m. A vertical array of 10 Wenglor laser particle counters (see Hugenholtz & Barchyn, 2011; Goossens et al., 2018) was used to monitor the height of the transport layer. The sensors were located between approximately 5 cm and 1 m above the surface, with the highest elevations varying slightly to ensure that at least 1 sensor was located higher than the model height. In addition, a time-lapse video with a 10s interval was made with a camera located at a height of 5 m, in order to record the experiment and to be able to identify interesting events such as streamers or natural bedforms migrating into the experiment area.

At the end of the day, the sedimentation and erosion patterns around the models were recorded and the models were removed. The sedimentation and erosion patterns were measured using structure-from-motion photogrammetry (see e.g. Van Puijenbroek et al., 2017). A telescopic stick was used to take photos all around the models, from a height of approximately 5 metres. These photos were computationally combined to form a digital elevation model (DEM) and orthophoto (a distortion-free top view) using Agisoft Photoscan (in December 2018 renamed to Agisoft Metascan). In Photoscan the accuracy was set to high for photo alignment and dense cloud generation, resulting in a horizontal resolution of approximately 2 mm for the DEM and orthophoto. The orthophoto and DEM were used to determine the erosion and deposition patterns and measure their dimensions.

The experiments were mainly conducted at the Sand Engine in the Netherlands (see Figure 4). At this mega beach nourishment, the beach is more than 500 metres wide, thus ensuring that there are always locations with large fetch lengths, independent of the wind direction. The median grain size is 335 µm (Hoonhout & De Vries, 2019). One experiment took place at the beach near Formerum, Terschelling. Here the beach is approximately 300 metres wide, so in combination with the almost shore-parallel wind that occurred enough for good Aeolian sand transport. Here, the median grain size is approximately 200 µm (Guillén &

Hoekstra, 1997). In total there were seven days during which sedimentation and erosion patterns around models were recorded. On average, 6 to 10 models (i.e. 6 to 10 stacks of different dimensions) were placed on the beach simultaneously, making for a total of 59 observations. Table 1 shows an overview of the conducted experiments.

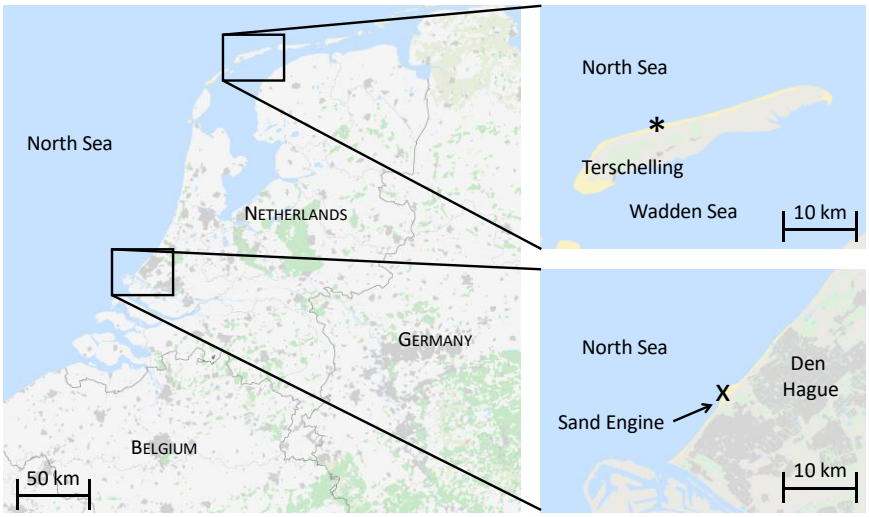

Figure 4: A map with the locations of the experiments, with the ✻ indicating the experiment at Terschelling and the X the experiments at the Sand Engine

Table 1. A Concise Overview of the Conducted Experiments

Date	**Location**	**Number of scale models**	**Wind speed [m/s]**	**Remarks**
29-05-2018	Terschelling	6	6.8	
11-10-2108	Sand Engine	9	5.9	Bed moist, less erodible
12-10-2018	Sand Engine	8	6.9	Bed moist, less erodible
23-10-2018	Sand Engine	10	9.5	
24-10-2018	Sand Engine	8	6.5	Light rain
19-11-2018	Sand Engine	9	7.6	
20-11-2018	Sand Engine	9	7.0	

Results

Figure 5 shows the sedimentation patterns around two models. The horseshoe-shaped deposition is clearly visible. At the right model, this horseshoe is almost continuous (nr 1, 4, 7): it is only interrupted at the upwind corners of the model. The model at the left is positioned slightly oblique to the wind, with the right side angled windward and the left side leeward. Here, the lateral horseshoe deposition (nr 4) is continuous at the right, but absent at the left. Zooming in on the models, some additional features become visible. At the left model, upwind inner deposition occurred (nr 3). Furthermore, the left model shows a hint of downwind inner deposition (nr 8), while the right model exhibits a clearer triangular-shaped downwind inner deposition. The left model also shows erosion to the outside of (what would be) the lateral horseshoe deposition (nr 10). This erosion, noticeable from the shells that remained after the sand was eroded, we term lateral outer erosion. The moist surface prevents the occurrence of upwind and lateral inner erosion, but both models show areas without deposition that might otherwise be eroded. Another interesting feature visible in both models is the double sedimentation ridge at the downwind edge of the upwind horseshoe deposition.

The patterns described above are fairly representative for patterns observed around other models and at other days. The upwind and downwind horseshoe deposition are present around virtually all models, with occasionally a larger distance between the downwind model corners and the start of the downwind horseshoe deposition (see Fig. 6a for an extreme case). The lateral horseshoe deposition shows more variation: often it is absent (Fig. 6a, 6b), sometimes it is present at one side (Fig. 5b, 6c, 6d) or at both sides (Fig. 5c: still interrupted at the upwind corners, Fig. 6e: fully present). For models oriented obliquely to the wind (due to inaccurate positioning or changing wind conditions), the lateral horseshoe deposition is often limited to the windward side. During three of the seven days, several models showed a double sedimentation ridge at the downwind edge of the upwind horseshoe deposition.

Upwind inner deposition occurred in slightly less than half of the cases (e.g. Fig. 6d). Downwind inner deposition occurred slightly more than half of the time. The presence or absence of this area was generally quite consistent for the different models tested during a day, with little effect from the model height. In case of models oriented obliquely to the wind, this downwind inner deposition occasionally formed one continuous deposition area together with the lateral leeward inner deposition (Fig. 6c, nr 6 and 8). Remarkably, all model set-ups used on the one day at Terschelling showed erosion instead of deposition directly downwind of the model (Fig. 6b). The upwind and lateral inner erosion also occurred a bit more than half of the time, with occurrence also depending on wind speed and surface erodibility. On 23-10-2018, the high wind speed (9.5 m/s) not

only caused inner erosion at the front and sides, but also undercutting at the corners (Fig. 6e and 6f). Lateral outer erosion was occasionally visible: around all of the models at 29-05-2018 and the majority of the models on 12-10-2018 (e.g. Fig 6b: with at the left side separate lateral outer and inner erosion and at the right side only lateral outer erosion).

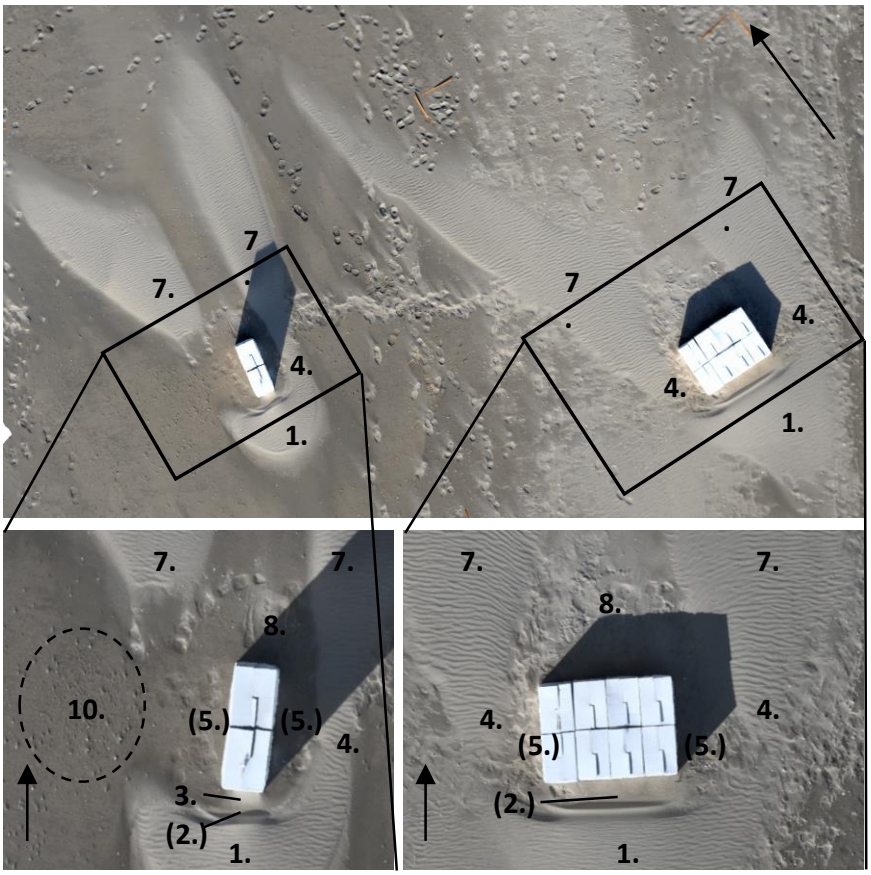

Figure 5: Orthophoto of the sedimentation and erosion around 2 models. Left model 1x2x2 boxes (32x100x70 cm), right model 4x2x1 boxes (128x100x35 cm), recorded at 12-10-2018. Numbers indicate sedimentation and erosion areas as presented in Figure 3, number between brackets indicate a lack of sedimentation on what is indicated as erosion area in figure 3. Arrows indicate wind direction. Number 10 indicates an area with erosion.

Figure 6: Notable erosion and sedimentation structures around scale models, with arrows indicating the wind direction. 6a) Orthophoto showing a large distance between the model and the start of the downwind horseshoe deposition. 6b) Orthophoto showing lateral inner and outer erosion and downwind inner erosion. 6c) Photo of a model oriented obliquely to the wind, showing lateral inner deposition 6d) Photo of model a oriented obliquely to the wind, showing upwind inner deposition and asymmetric lateral deposition. 6e) Photo showing continuous lateral deposition. 6f) Zoom of 6e, showing erosion around model and under model corners.

Discussion

The deposition and erosion patterns found in the experiment are similar to the snow accumulation patterns around buildings reported in literature. However, there are some differences. The negative effect of the wind speed on the presence of lateral horseshoe deposition, as reported in Liu et al. (2018), is not confirmed. On the contrary, continuous lateral horseshoe deposition at both sides of the model was especially present at the day with the highest wind speed (9.5 m/s). At low wind speeds, Liu et al further observed continuous upwind snow deposition from the horseshoe to the building front. In our experiments, there was an area showing either a lack of deposition or even erosion between the upwind horseshoe deposition and the front of the model. However, the lowest wind speed that Liu et al. observed (1.5 m/s) was lower than the critical wind speed, so no erosion could occur. At this wind speed, snow transport consists of the convection of snow fall. This snow fall is blown against the front of the building, but the reverse flow of the horseshoe vortex lacks the strength to cause erosion. At the beach, sand/snow fall does not exist as supply mechanism. Hence, sand transport can only occur at higher wind speeds that induce motion at the bed. At this wind speed, the reverse flow in front of our models seemed to cause an area without sedimentation (or even erosion) between the upwind horseshoe deposition and the model front.

A new observation in this experiment is the occurrence of erosion further outward from the sides of the model. In some cases a distinct lateral outer erosion area formed outside of the normal horseshoe sedimentation. In other cases, erosion already started near the model, but extended further than where the horseshoe sedimentation would be expected to form.

The experiment also showed the effect of the wind direction. The models that were oriented obliquely to the wind generally tended to only show lateral horseshoe deposition at the windward side, and not at the leeward side. This agrees well with the pattern that Liu et al. (2018) found for snow accumulation around a cube oriented slightly oblique to the wind under higher wind speeds (10° angle, 4.5 m/s wind speed). However, the presence and clearness of the lateral horseshoe deposition we observed, also showed strong variation for models oriented perpendicular to the wind, so the interplay between orientation, wind speed and lateral horseshoe deposition remains a subject for further research.

In this paper, we described generic patterns of deposition and erosion around scale models of buildings. The wind speed and differences in the erodibility of the bed are only mentioned where especially relevant. A more systematic analysis of the effect of these factors on the type of sedimentation and erosion patterns should be conducted in the future. This is especially relevant for the lateral horseshoe

deposition and downwind inner deposition, for which previous experiments on snow accumulation (e.g. Thiis, 2003; Liu et al., 2018) suggest an effect from the wind speed. Furthermore, the effect of the model size and shape on the dimensions of the sedimentation and erosion patterns will be examined in future research.

Conclusions

To determine the Aeolian erosion and deposition patterns around buildings on the beach, a scale experiment was conducted. This experiment, conducted at the beach, showed that the deposition and erosion patterns formed by sand are quite similar to the patterns of snow accumulation around buildings. Deposition patterns follow the horseshoe vortex that the wind forms around a building. The deposition area upwind of the building and the deposition tails downwind of the building (downwind horseshoe deposition) are almost always present if the wind is strong enough to cause sand transport. The presence of horseshoe deposition to the side of the building (lateral horseshoe deposition) and of deposition and erosion between the horseshoe and the building itself is more variable, and depends on wind speed, wind direction, and the erodibility of the bed. In contrast to earlier research on snow accumulation, we did not observe a clear effect of the wind speed on the lateral horseshoe deposition. In addition, the upwind snow deposition continued up to the building front for the lowest wind speeds, while our upwind deposition was always located some distance upwind of the building. A further analysis of the experimental data is needed to draw more quantitative conclusions on the effect of building size and shape on the dimensions of the sedimentation and erosion patterns.

Acknowledgements

This research forms part of the ShoreScape project (Sustainable co-evolution of the natural and built environment along sandy shores), funded by the Netherlands Organization for Scientific Research (NWO), contract number ALWTW.2016.036, co-funded by Hoogheemraadschap Hollands Noorderkwartier and Rijkswaterstaat, and in kind supported by Deltares, Witteveen&BOS, and H+N+S. We also want to thank Rijkswaterstaat for the logistic support during the experiment at the Sand Engine. Furthermore, we thank Jan Willem van Dokkum for his great help during the preparation and execution of the experiments. In addition, we are grateful to Janneke van Bergen, Sara Dionísio António, Weiqiu Chen, Joost Kranenborg, Mariëlle Rotteveel, Sam de Roover, Ton van der Heide and the organization of the Oerol festival for their assistance with the experiments.

References

Carter, R. W. G. (1991). Near-future sea level impacts on coastal dune landscapes. *Landscape Ecology, 6*(1), 29-39. doi:10.1007/bf00157742

De Winter, R. C., & Ruessink, B. G. (2017). Sensitivity analysis of climate change impacts on dune erosion: case study for the Dutch Holland coast. *Climatic Change, 141*(4), 685-701. doi:10.1007/s10584-017-1922-3

Duthinh, D., & Simiu, E. (2011). The Use of Wind Tunnel Measurements in Building Design. In J. C. Lerner (Ed.), *Wind Tunnels and Experimental Fluid Dynamics Research* (pp. 282-300): InTech.

Goossens, D., Nolet, C., Etyemezian, V., Duarte-Campos, L., Bakker, G., & Riksen, M. (2018). Field testing, comparison, and discussion of five aeolian sand transport measuring devices operating on different measuring principles. *Aeolian Research, 32*, 1-13. doi:10.1016/j.aeolia.2018.01.001

Guillén, J., & Hoekstra, P. (1997). Sediment Distribution in the Nearshore Zone: Grain Size Evolution in Response to Shoreface Nourishment (Island of Terschelling, The Netherlands). *Estuarine, Coastal and Shelf Science, 45*(5), 639-652. doi:10.1006/ecss.1996.0218

Hall, C. M. (2001). Trends in ocean and coastal tourism: the end of the last frontier? *Ocean & Coastal Management, 44*(9), 601-618. doi:10.1016/S0964-5691(01)00071-0

Hoonhout, B., & De Vries, S. (2019). Simulating spatiotemporal aeolian sediment supply at a mega nourishment. *Coastal engineering, 145*, 21-35. doi:10.1016/j.coastaleng.2018.12.007

Hoonhout, B. M., & Waagmeester, N. (2014). *Invloed van strandbebouwing op zandverstuiving, Een verkenning naar methoden, meetgegevens en modellen*. Delft: Deltares.

Hugenholtz, C. H., & Barchyn, T. E. (2011). Laboratory and field performance of a laser particle counter for measuring aeolian sand transport. *Journal of Geophysical Research: Earth Surface, 116*(F1). doi:10.1029/2010JF001822

Hunt, J. (1971). The effect of single buildings and structures. *Phil. Trans. R. Soc. Lond. A, 269*(1199), 457-467.

Jackson, N. L., & Nordstrom, K. F. (2011). Aeolian sediment transport and landforms in managed coastal systems: A review. *Aeolian Research, 3*(2), 181-196. doi:10.1016/j.aeolia.2011.03.011

Keijsers, J. (2015). *Modelling foredune dynamics in response to climate change.* Wageningen University.

Liu, M., Zhang, Q., Fan, F., & Shen, S. (2018). Experiments on natural snow distribution around simplified building models based on open air snow-wind combined experimental facility. *Journal of Wind Engineering and Industrial Aerodynamics, 173*, 1-13. doi:10.1016/j.jweia.2017.12.010

Malavasi, M., Santoro, R., Cutini, M., Acosta, A. T. R., & Carranza, M. L. (2013). What has happened to coastal dunes in the last half century? A multitemporal

coastal landscape analysis in Central Italy. *Landscape and Urban Planning, 119*, 54-63. doi:10.1016/j.landurbplan.2013.06.012

Martinuzzi, R., & Tropea, C. (1993). The Flow Around Surface-Mounted, Prismatic Obstacles Placed in a Fully Developed Channel Flow (Data Bank Contribution). *Journal of Fluids Engineering, 115*(1), 85-92. doi:10.1115/1.2910118

Moreno, A., & Amelung, B. (2009). Climate Change and Coastal & Marine Tourism: Review and Analysis. *Journal of Coastal Research*, 1140-1144.

Morton, R. A., Paine, J. G., & Gibeaut, J. C. (1994). Stages and Durations of Post-Storm Beach Recovery, Southeastern Texas Coast, USA. *Journal of Coastal Research, 10*(4), 884-908.

Nordstrom, K. F. (2000). *Beaches and dunes of developed coasts*: Cambridge University Press.

Nordstrom, K. F., & James, M. M. (1985). The Effects of Houses and Sand Fences on the Eolian Sediment Budget at Fire Island, New York. *Journal of Coastal Research, 1*(1), 39-46.

Oikawa, S., & Tomabechi, T. (2000). Daily observations of snowdrifts around a model cube. *Fourth Conference of Snow Engineering*, 137-141.

Peterka, J. A., Meroney, R. N., & Kothari, K. M. (1985). Wind flow patterns about buildings. *Journal of Wind Engineering and Industrial Aerodynamics, 21*(1), 21-38. doi:10.1016/0167-6105(85)90031-5

Schlacher, T. A., Schoeman, D. S., Dugan, J., Lastra, M., Jones, A., Scapini, F., & McLachlan, A. (2008). Sandy beach ecosystems: key features, sampling issues, management challenges and climate change impacts. *Marine Ecology, 29*(s1), 70-90. doi:10.1111/j.1439-0485.2007.00204.x

Smith, A. B., Jackson, D. W. T., Cooper, J. A. G., & Hernández-Calvento, L. (2017). Quantifying the role of urbanization on airflow perturbations and dunefield evolution. *Earth's Future, 5*(5), 520-539. doi:10.1002/2016ef000524

Thiis, T. K. (2003). Large scale studies of development of snowdrifts around buildings. *Journal of Wind Engineering and Industrial Aerodynamics, 91*(6), 829-839. doi:10.1016/S0167-6105(02)00474-9

Thiis, T. K., & Gjessing, Y. (1999). Large-scale measurements of snowdrifts around flat-roofed and single-pitch-roofed buildings. *Cold Regions Science and Technology, 30*(1), 175-181. doi:10.1016/S0165-232X(99)00021-X

Van Puijenbroek, M. E. B., Nolet, C., De Groot, A. V., Suomalainen, J. M., Riksen, M. J. P. M., Berendse, F., & Limpens, J. (2017). Exploring the contributions of vegetation and dune size to early dune development using unmanned aerial vehicle (UAV) imaging. *Biogeosciences, 14*(23), 5533-5549. doi:10.5194/bg-14-5533-2017

White, B. R. (1996). Laboratory simulation of aeolian sand transport and physical modeling of flow around dunes. *Annals of Arid Zone, 35*(3), 187-213.